CLRC
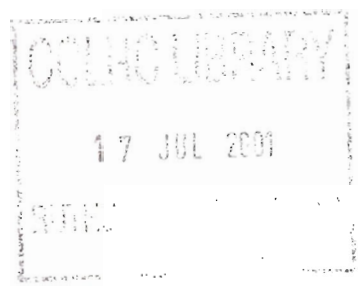
Orbital Properties of Vanadium Ions in Magnetically Ordered V_2O_3

S W Lovesey K S Knight and D S Sivia

16th July 2001

ORBITAL PROPERTIES OF VANADIUM IONS
IN MAGNETICALLY ORDERED V_2O_3

S. W. Lovesey, K. S. Knight and D. S. Sivia*

1. INTRODUCTION

Vanadium sesquioxide (V_2O_3) displays a number of electronic, magnetic and structural properties that are challenging to interpret and explain[1-7]. At room temperature V_2O_3 has the corundum structure with space group $R\bar{3}c$, and it is metallic and paramagnetic. On reducing the temperature the corundum structure distorts to a monoclinic structure with space group $I2/a$. The structural transition in the temperature range 150 – 160K is strongly first-order and ferroelastic. Accompanying the transition are a change from metallic to insulating behaviour and the onset of antiferromagnetic order[3]. The metal-insulator transition is viewed as a classic Mott transition, in which spin and orbital degrees of freedom are independent.

Recently, results from resonant x-ray Bragg diffraction experiments[8-10] have added to the wealth of knowledge about V_2O_3. We put forward a detailed theoretical explanation of some key aspects of the observed x-ray diffraction pattern[11] in which intensity is enhanced by the resonance at the K-edge of a vanadium ion. The success of our model in explaining the resonant x-ray diffraction data permits us to draw specific conclusions about the orbital magnetization present in V_2O_3.

The resonance enhanced intensity is related to properties of the valence shell that accommodates the photo-ejected core electron in the intermediate state of the elastic scattering process. Absorption at the K-edge and an electric-dipole event (E1) gives access to valence states with atomic p-like character, and an electric quadrupole event (E2) at the same edge gives access to d-like states (1s $\rightarrow$ 3d). We analyse in terms of a pure E2 event diffraction data collected with the primary energy tuned to a feature in the pre-edge (5.464 keV and λ = 2.27Å) of the vanadium K-shell. The associated Bragg intensity is therefore attributed directly to properties of the 3d-shell of a vanadium ion. As a function of the primary energy, the observed intensity is adequately described by a

*ISIS Facility, Rutherford Appleton Laboratory, Oxfordshire, OX11 0QX, UK.

single oscillator. In this instance, we can confidently ascribe the intensity to orbital degrees of freedom and spin degrees of freedom are not explicitly contributing.

The data of interest has been gathered for Bragg reflections that are forbidden by the space group, and often called charge-forbidden reflections. In general, such reflections are due to spatial anisotropy in the charge distribution or a long-range magnetic order that is not indexed on the chemical structure. When long-range magnetic order is absent, the diffraction at charge-forbidden reflections is usually referred to as Templeton-Templeton scattering[12, 13]. Intensities measured for different settings of the crystal rotated about the Bragg wavevector can provide direct information on the nature of the anisotropy and spatial symmetry. Should the Bragg wavevector coincide with an axis of rotation symmetry the azimuthal-angle (ψ) meshes with the rotational periodicity, and the Bragg intensity displays a periodicity in ψ equal to twice the degree of the axis of rotation[14, 15]. Such a configuration can be achieved in diffraction from the corundum structure[11, 14] and the observed azimuthal-angle scan is six-fold periodic. Broadly speaking, complexity in azimuthal-angle scans observed for magnetically ordered V_2O_3[8-10] is due to the low spatial symmetry of the monoclinic structure adopted by the crystal. While the symmetry of the site occupied by a resonant vanadium ion carries an imprint of a three-fold axis of rotation, monoclinic Bragg wavevectors generally do not coincide with the trigonal axis of the corundum structure and it is this mismatch, between the wavevectors and the axis of rotation, that is largely responsible for the seemingly complex pattern of the azimuthal-angle scans.

There are two main ingredients in the calculated structure factors. First, knowledge of the chemical and magnetic structures. Information on the crystal structure, which is based on observations reported by Dernier and Marezio[2], is gathered in section 2 together with the configuration of magnetic moments[3]. The second ingredient is a model of resonance-enhanced Bragg diffraction. We employ an atomic model which should be adequate for a one-component intensity profile like the ones observed with V_2O_3 at the vanadium K-shell pre-edge[8, 9]. After adopting a single oscillator to describe the intensity profile the amplitude attached to the oscillator can be calculated without further approximation.[16] The atomic model for the event 1s $\rightarrow$ 3d, which is of interest to us here, shows that the amplitude is constructed from spherical tensors that describe the orbital properties of the 3d-shell. After putting together the two ingredients it only remains to describe the geometry of the experiment, namely, the orientation of the crystal (a function of the azimuthal angle) in the frame of reference used for the polarization and wavevector of the primary and diffracted beams of x-rays. The calculation of structure factors for unrotated ($\sigma'\sigma$) and rotated ($\pi'\sigma$) channels of scattering is outlined in section 3 together with examples of our interpretation of x-ray diffraction data. Thereafter, in section 4, we characterize the orbital properties of a vanadium ion by exploiting our success with the interpretation. Our conclusions are found in section 5.

2. CHEMICAL AND MAGNETIC STRUCTURES

At room temperature vanadium sesquioxide has a trigonal (corundum) structure with space group 167 ($R\bar{3}c$). Lowering the temperature of the material induces distortions which include tilting of the trigonal (hexagonal-c) axis and reduction of the point-group symmetry of sites occupied by vanadium ions from 3(C_3) to that of no symmetry.
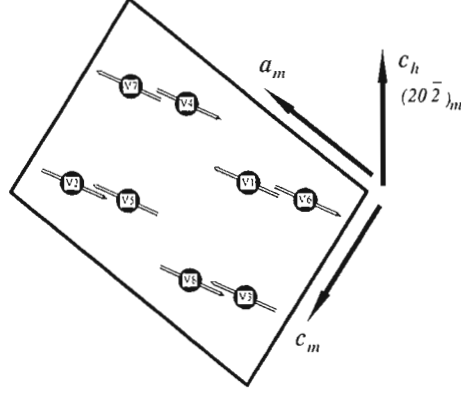
Figure 1. Positions of the eight vanadium ions in the monoclinic unit cell together with the configuration of their magnetic moments which lie in the $\mathbf{a}_m - \mathbf{c}_m$ plane of the diagram. The monoclinic Bragg wavevector $(20\bar{2})_m$ is parallel to the trigonal axis $\mathbf{c}_h$, and $\mathbf{b}_m$ is normal to the plane of the diagram and parallel to $\mathbf{a}_h$.

The space group of the low temperature monoclinic structure is number $15(I2/a)$ in which vanadium ions occupy sites 8 (f). This is a body-centred cell and Bragg wavevectors $\tau_m(hkl)$ for charge reflections have the necessary condition $h + k + l$ an even integer. (Miller indices h, k and l are integers.) The antiferromagnetic configuration of vanadium magnetic moments, displayed in Fig. 1, consists of sheets of moments with ferromagnetic alignment within $(010)_m$ layers, or hexagonal (110) layers, and moment reversal between adjacent layers. The moments are orientated along some easy-axis in these layers, and we take ϕ as the canting angle with respect to the trigonal axis.

The trigonal basis vectors are $\mathbf{a}_h = a(1, 0, 0)$, $\mathbf{b}_h = a(-\frac{1}{2}, \frac{1}{2} \sqrt{3}, 0)$ and $\mathbf{c}_h = c(0, 0, 1)$ and the volume of the unit cell $= a^2 c \sqrt{3} / 2$. Following Dernier and Marezio[2] in the use of an I - centred cell, from these vectors we generate monoclinic basis vectors $\mathbf{a}_m = (0, 2a/\sqrt{3}, c/3)$, $\mathbf{b}_m = \mathbf{a}_h$ and $\mathbf{c}_m = (0, a/\sqrt{3}, -c/3)$, and the volume of the cell $= a^2 c / \sqrt{3}$. The corresponding Bragg wavevector $\tau_m(hkl) \equiv (hkl)_m$ is,

$$\tau_m(hkl) = (k, (h+l)/\sqrt{3}, (h-2l)a/c)/a. \tag{1}$$

We note that $(l0\bar{l})_m$ is parallel to $\mathbf{c}_h$ and $(2lkl)_m$ is normal to $\mathbf{c}_h$.

Referring to Fig. 1, the position coordinates of vanadium ions labelled (1) and (5) are (x, y, z) and $(-x, -y, -z)$, respectively, with $x = 0.3439$, $y = 0.0012$ and $z = 0.2993$[2]. The positions of the pair (2) and (6) are related by a body-centre translation to the pair (1) and (5). The position coordinates of (3) and (7) are $(\frac{1}{2} -x, y, -z)$ and $(\frac{1}{2} +x, -y, z)$, respectively, and the pairs (4) and (8), and (3) and (7) are related by the body-centre translation. The body-centre translation $(\frac{1}{2},\frac{1}{2},\frac{1}{2})_m = (1, \sqrt{3}, 0)a/2$ and $(\frac{1}{2},\frac{1}{2},\frac{1}{2})_m \cdot \tau_m(hkl) = \frac{1}{2}(h + k + l)$. In writing out spatial phase factors in the structure factor one finds two angles $v = 2\pi(x, y, z)_m \cdot \tau_m(hkl) = 2\pi(xh + yk + zl)$ and $\varepsilon = 4\pi yk \sim 0$.

3. THE STRUCTURE FACTOR FOR BRAGG DIFFRACTION BY MAGNETICALLY ORDERED V_2O_3

As a function of the energy of the primary x-rays, the observed intensity of diffraction from V_2O_3 which is enhanced by electric-quadrupole (E2) resonance has a distinct shape[8, 9] which is adequately described by a single oscillator. In this treatment, the integrated intensity is calculated without approximation[16], and for a pure E2 absorption event 1s $\rightarrow$ 3d the intensity is proportional to the orbital moments of the 3d valence shell. The orbital moments are represented by atomic tensors $\langle \mathbf{T}^{(K)} \rangle$ of rank $K = 0, 1, 2, 3$ and 4. In the structure factor, which is a scalar quantity, atomic tensors appear in a scalar product with a tensor, denoted by $\mathbf{H}^{(K)}$, that describes the conditions of the primary and diffracted beams of x-rays. It is convenient to consider the quantity,

$$\Psi_Q^{(K)} = \sum_{\mathbf{d}} \ <T_Q^{(K)}(\mathbf{d})> \exp(i\tau \cdot \mathbf{d}), \tag{2}$$

where $-K \leq Q \leq K$, $\mathbf{d}$ defines the position of a resonant vanadium ion in the unit cell and τ is the Bragg wavevector for the reflection in question. With this notation the structure factor is [16, 17],

$$F(\tau) = \sum_K (2K+1)^{1/2} \mathbf{H}^{(K)} \cdot \mathbf{\Psi}^{(K)} = \sum_{K,Q} (2K+1)^{1/2} (-1)^Q H_{-Q}^{(K)} \Psi_Q^{(K)} . \tag{3}$$

The components $H_Q^{(K)}$ for unrotated $(\sigma'\sigma)$ and rotated $(\pi'\sigma)$ radiation are tabulated [17]. In Equ. (3) the tensor $\mathbf{H}^{(K)}$ and $\Psi^{(K)}$ are evaluated in the coordinate system that defines the experimental geometry. Referring to Fig. 2, σ-polarization is perpendicular to the plane of scattering and parallel to the z-axis, and $\hat{\mathbf{q}} - \hat{\mathbf{q}}' = -2\sin\theta\,\hat{\mathbf{x}}$ and $\hat{\mathbf{q}} + \hat{\mathbf{q}}' = 2\cos\theta\,\hat{\mathbf{y}}$ where θ is the Bragg angle.
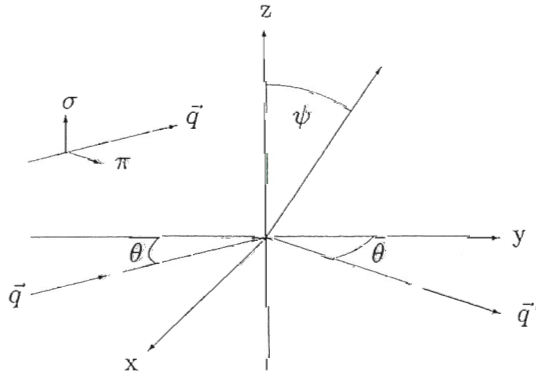

Figure 2. The orthogonal states of polarization in the primary beam of x-rays with σ-polarization normal to the plane of scattering defined by the primary (**q**) and diffracted (**q**′) wavevectors. X-rays are deflected through an angle 2θ and $\tau_m = \mathbf{q} - \mathbf{q}'$. Orthogonal axes (x, y, z) are related to the geometry of the experiment; the x-axis is parallel to $-\tau_m$ and the z-axis is normal to the plane of scattering and parallel to σ-polarization. An azimuthal-angle scan is rotation of the crystal by ψ about τ_m, and the origin $\psi = 0$ is defined by a specified plane normal to the plane of scattering.

We find it convenient initially to consider $\Psi_Q^{(K)}$ with respect to a second set of orthogonal axes (x,y,z) that include $\mathbf{a}_h = (a,0,0) = \mathbf{b}_m$ and $\mathbf{c}_h = (0,0,c)$. Thereafter we apply to $\Psi_Q^{(K)}$ rotations that describe the orientation of the crystal in the coordinates of the experimental geometry that apply to $\mathbf{H}^{(K)}$.

Following the discussion in section 2, the chemical environments of ions in the pairs (1) & (2), (5) & (6), (7) & (8) and (3) & (4) are identical. Moreover, the axes of quantization of ions in a pair are oppositely aligned and, in consequence, their atomic tensors differ by a phase factor $(-1)^K$. Odd-rank tensors are purely magnetic and $\langle \mathbf{T}^{(1)} \rangle = \langle \mathbf{L} \rangle / \sqrt{30}$ and $\langle \mathbf{T}^{(3)} \rangle = \langle \Lambda \rangle / 3\sqrt{70}$ where $\langle \mathbf{L} \rangle$ and $\langle \Lambda \rangle$ are, respectively, the orbital magnetic moment and the orbital octupole moment of the 3d-valence shell of a resonant vanadium ion. Vanadium ions at sites (1) & (5) are related by inversion. The atomic tensor is unchanged by inversion and thus $< T_Q^{(K)}(1) > = < T_Q^{(K)}(5) >$. A similar relation holds for (3) & (7).

Ions at sites (1) & (7) are related by an a-glide that includes reflection in the $\mathbf{a}_m$ - $\mathbf{c}_m$ plane, which is normal to $\mathbf{a}_h = \mathbf{b}_m$. Reflection in the $\mathbf{a}_m$ - $\mathbf{c}_m$ plane amounts to the change $x \rightarrow -x$, and with it $< T_Q^{(K)} > \rightarrow (-1)^K < T_{-Q}^{(K)} >$. For $K = 1$ $(L_x, L_y, L_z) \rightarrow (L_x, -L_y, -L_z)$, so that reflection in the $\mathbf{a}_m$ - $\mathbf{c}_m$ plane is accompanied by a change in the orientation of the orbital magnetization. The configuration of moments determined by Moon[3] is preserved if the polarity of the local field is now reversed, leading to $(L_x, -L_y, -L_z) \rightarrow (-L_x, L_y, L_z)$, for according to Moon $\langle L_x \rangle = 0$ and the moments are confined to the $\mathbf{a}_m$ - $\mathbf{c}_m$ plane. Reversing the polarity of the local field, which is sometimes described as time-reversal, introduces in the atomic tensor a phase factor $(-1)^K$. The appropriate relation between tensors at sites (1) and (7) is seen to be the union of reflection in the $\mathbf{a}_m$ - $\mathbf{c}_m$ plane and time-reversal, and our discussion leads to the result $\langle T_Q^{(K)}(7) \rangle = \langle T_{-Q}^{(K)}(1) \rangle$; for simplicity of notation, we hereafter write $< T_Q^{(K)} > = < T_Q^{(K)}(1) >$.

In the monoclinic structure, sites occupied by the vanadium ions possess no spatial symmetry and one can choose any set of axes for the associated atomic tensors. When proceeding from the corundum structure to the monoclinic one the average vanadium-oxygen distance remains essentially constant. This aspect of the structural transition, and others mentioned in section 2, indicate that in the monoclinic structure the potential field experienced by a vanadium ion is principally referred to the trigonal axis, $\mathbf{c}_h$, and the field is almost subject to the requirement of a three-fold axis of rotation. An atomic tensor invariant with respect to a three-fold rotation is zero unless the projection index Q has the values 0 or ± 3. Additions to the potential field, which reduce the symmetry from C_3 to one of no spatial symmetry, lift the restriction on the allowed values of Q.

3.1 Templeton-Templeton scattering

For the model of V$_2$O$_3$ we have described, in the previous section, $\Psi_Q^{(K)}$ can be different from zero for even values of $K+(h+k+l)$, so there is a selection rule on scattering that links the sum of Miller indices and the rank of atomic tensors. In this sub-

section we interpret data indexed by even $(h+k+l)$ and tensors in the corresponding structure factor have an even rank. The appropriate expression for $\Psi_Q^{(K)}$ is,

$$\Psi_Q^{(K)} = 4\cos(\nu)\{<T_Q^{(K)}> +(-1)^h <T_{-Q}^{(K)}>\}. \tag{4}$$

Note that for h odd the contributing tensors have rank $K = 2$ and $K = 4$ and there is no contribution in $\Psi_Q^{(K)}$ with $K = 0$ or $Q = 0$. Diffraction indexed by even $(h+k+l)$ and odd h is Templeton-Templeton scattering.

An example of such scattering has been observed at $(10\bar{1})_m$. Because this Bragg wavevector is parallel to our chosen principal axis $\mathbf{c}_h$ an azimuthal-angle scan, which is rotation of the crystal around the Bragg wavevector, incorporates what amounts to another selection rule that limits harmonics of the azimuthal angle ψ to values set by the projection index Q of atomic tensors. In consequence, the structure factor that describes an azimuthal-angle scan at $(10\bar{1})_m$ is a linear combination of $<T_Q^{(K)}>\cos(Q\psi)$.

A confrontation between predictions of the theory and the data requires the input of several parameters. Some can be derived from geometrical considerations, such as Euler angles for orienting the crystal in the geometry of the experiment and the Bragg angle, and are believed to be estimated fairly well; others are experimental in nature, particularly the zero-setting for the azimuthal angle, but are thought to be calibrated reasonably well; some stem from material properties, and little is known about their values a priori. These varying degrees of uncertainty are easily taken into account within the Bayesian framework of data analysis[18] and, with suitable commonly-used simplifying assumptions, lead to a somewhat generalized form of least-squares: in addition to a quadratic cost function for a mismatch with the measurements, there is also a penalty for deviating from those parameter-values within the theory which are thought to be known fairly well. The best fit to data (e.g. Fig. 3) utilizes a robust simplex algorithm[19] for carrying out the (local) optimization.

Our interpretation of the azimuthal-angle scan at $(10\bar{1})_m$ is illustrated in Fig. 3. The data are collected in the rotated $(\pi'\sigma)$ channel of scattering. The material properties that enter our interpretation are $<T_Q^{(2)}>$ with $Q = 1$ and 2 and $<T_Q^{(4)}>$ with $Q = 1, 2, 3$ and 4. We find that the coeffficients of $\cos(\psi)$ and $\cos(3\psi)$, by far, are the largest, and in creating Fig.3 $<T_4^{(4)}>$ is set equal to zero. One finds the coefficients of $\cos(3\psi)$ and $\cos(2\psi)$ differ by more than an order of magnitude, and the coefficients of $\cos(3\psi)$ and $\cos(\psi)$ are in the ratio ~ 0.2.

3.2 Magnetic scattering

Here we are concerned with space-group forbidden reflections indexed by odd $(h+k+l)$. The corresponding atomic tensors are odd with respect to their rank and they vanish with loss of long-range magnetic order. The structure factor is constructed from $\Psi_Q^{(K)}$ defined in Equ. (4). (The diffraction pattern observed when neutrons are scattered
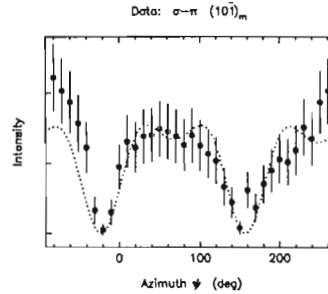
Figure 3. Data gathered in the rotated polarization channel at the $(10\bar{1})_m$ reflection from V$_2$O$_3$ with 2.8% Cr doping, held at a temperature of 100K. The continuous curve is generated from, Equ. (4) with a Bragg angle $\theta = 14.1°$ ($\lambda = 2.27$Å). The origin of the azimuthal-angle scan is specified by a plane in reciprocal − space normal to the plane of scattering. The plane in question is defined by $(10\bar{1})_m$ and $(211)_m$ and on our scale for ψ the origin is at − 60°.

by magnetically ordered V$_2$O$_3$ is indexed by odd $(h+k+l)$ and even h.) Figure 4 contains examples of our interpretations of resonant x-ray Bragg diffraction.

We have successfully compared calculated intensities with data gathered in azimuthal-angle scans at space-group forbidden reflections $(2\bar{2}1)_m$, $(111)_m$ and $(30\bar{2})_m$. As a function of the primary energy of the x-rays the signal observed at 5.464 keV is fully consistent with a single-oscillator model. From this premiss, the x-ray experiments in question reveal exclusively the orbital magnetization of V$_2$O$_3$, and quantities not directly obtainable with other experimental techniques.

Calculated structure factors conform to established chemical and magnetic structural properties. At space-group forbidden reflections, the structure factors contain the following additional features.

(a) Reflections are purely magnetic, being associated with atomic moments of the vanadium 3d-valence shell that are odd with respect to the reversal of time. In general, such moments vanish with the loss of long-range magnetic order. Our prediction for V$_2$O$_3$ is borne out in experiments which show that intensities decrease with increasing temperature, and vanish at the Néel temperature.

(b) A selection rule on the order of the electric absorption event and Miller indices $h\,k\,l$. With $h + k + l$ odd (a space-group forbidden reflection) reflections with h odd do not contain a contribution from an E1 (electric dipole) event, and the finding is in accord with observations. In the reported calculation, the selection rule stems from the actual configuration of magnetic moments and the fact that they are contained in the $\mathbf{a}_m$ - $\mathbf{c}_m$ plane. The same fact is utilized in arriving at the general form of the structure factor, based on the established chemical structure augmented by the operation of time reversal.

(c) With h odd diffraction is by anisotropic components of the orbital octupole moment of a vanadium ion. Such diffraction might be regarded as the magnetic equivalent of Templeton and Templeton scattering from a charge distribution.
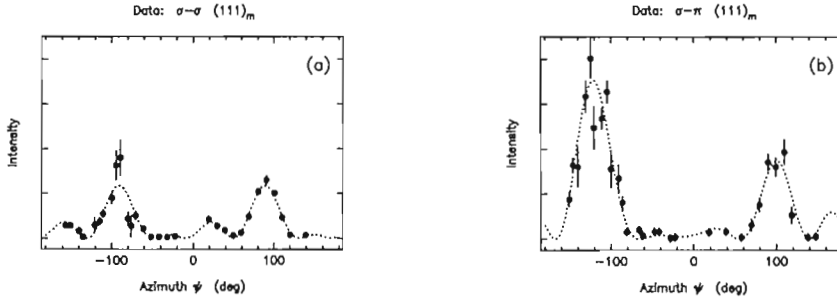
Figure 4. Data on Cr-doped V_2O_3 held at temperature = 0.55 T_N = 100K, and τ_m = $(111)_m$ with θ = 20.8°. From data in the unrotated channel we find r = 0.33 ± 0.04 and t = – 0.35 ± 0.15, and from data in the rotated channel we find r = 0.36 ± 0.02 and t = – 1.00 ± 0.13.

(d) Intensities with h even can be used to determine the canting angle, ϕ, of the magnetic easy-axis. Our analysis of data gathered at the pre-edge (5.464 keV) and $(2\bar{2}1)_m$ gives $\phi \sim 70°$ and the value is consistent with the analysis of intensities observed in magnetic neutron diffraction[3]. This outcome at the pre-edge, and related success in explaining other features, confirm that it is due mainly to an E2 resonance event.

(e) As a function of the azimuthal-angle the calculated intensity in the channel with unrotated polarization ($\sigma'\sigma$) is two-fold periodic. This prediction and additional detail in calculated ($\sigma'\sigma$) azimuthal-angle scans is found in intensities collected at Bragg reflections $(2\bar{2}1)_m$, $(111)_m$ and $(30\bar{2})_m$.

(f) In general, the dependence on azimuthal-angle of intensities in the rotated channel ($\pi'\sigma$) show no systematic features. With h odd the ($\pi'\sigma$) azimuthal-angle scans have a quite complicated pattern which essentially reflects the low symmetry (monoclinic) of the crystal below the Néel temperature.

4. A CHARACTERIZATION OF THE ORBITAL PROPERTIES OF A V ION

We construct a model wavefunction to characterize the orbital properties of a vanadium ion deduced from our interpretation of data collected on magnetically ordered V_2O_3 by resonant x-ray diffraction. The model is based on the ^3F term of V^{3+} ($3d^2$), and orbital components $|M\rangle$ with $-3 \leq M \leq 3$. Should the V ion occupy a site that contains an axis of three-fold rotation symmetry (C_3) components in the wavefunction must differ by $M = \pm 3$, and $\langle T_Q^{(K)} \rangle$ can be different from zero for $Q = 0$ and ± 3. In the absence of spatial symmetry no selection rules operate on M and all Q are allowed. On using a wavefunction,

$$|G\rangle = a|-2\rangle + b|-1\rangle + c|0\rangle + d|1\rangle, \tag{5}$$

non-zero values of b and c represent the influence of reducing the V ion site symmetry from C_3 to that of no spatial symmetry. Our interpretation of the data can be characterized by $|G>$ on taking a, b and d purely real and $c = c'+ic''$, and the normalized wavefunction contains four independent coefficients.

In addition to normalization of $|G>$, coefficients in the wavefunction are constrained by requiring the orbital magnetic moment to lie in the plane $a_m - c_m$ and enclose an angle ϕ with c_h. The orbital magnetic moment $< L_0 >_m$ satisfies,

$$< L_0 >_m \cos \phi = d^2 - b^2 - 2a^2, \tag{6}$$

together with,

$$ab \sqrt{5} + c'(b+d) \sqrt{6} = 0. \tag{7}$$

The material quantities that enter our interpretation of data collected at magnetic reflections include ratios of components of the octupole moment, namely,

$$r = \sqrt{3/5} < \Lambda_{+1} >' / < \Lambda_{+3} >' = b/2d, \tag{8}$$

$$t = \sqrt{6} < \Lambda_{+2} >'' / < \Lambda_{+3} >' = -c'' \sqrt{3} /d \tag{9}$$

$$\text{and,} \quad < \Lambda_0 >_m = 3 (a^2 + b^2 - d^2) \cos \phi (3 - 5 \cos^2 \phi)/2. \tag{10}$$

Other quantities of interest are components of the quadrupole moment, e.g.,

$$< Q_0> = 3\{3(b^2 + d^2) + 4 |c|^2\}/10. \tag{11}$$

There remains the question as to how well the experimental data constrains the three unknown coefficients in $|G>$. If the answer is fairly tightly, then we can make useful predictions about material quantities, like $<Q_0>$, which do not appear in structure factors for space-group forbidden reflections.

The coefficients are related to quantities inferred from x-ray and neutron diffraction data. These quantities are ϕ, r, t, $< L_0 >_m$ and the ratio $< \Lambda_0 >_m /3 < L_0 >_m$. We have two, or more, estimates of ϕ, r, t, $< L_0 >_m$ and the ratio $< \Lambda_0 >_m /3 < L_0 >_m$, and wish to know what restrictions these impose on the allowed values of a, b and d, say. Before proceeding to that, however, let us first consider the intermediate step of combining the different estimates of the same quantity into a single entity. For example, what does $r = 0.81 \pm 0.11$, 1.24 ± 0.24, 0.33 ± 0.04 and 0.36 ± 0.02 tell us about the possible value of r? Well, assuming independence between the four relevant data sets, the usual elementary analysis[18], leading to a weighted mean combination, yields the summary $r = 0.37 \pm 0.02$. While this result is understandable given the large spread in the size of the error bars on the four estimates of r, it does not sit well with our common sense intuition. A more reasonable representation of our state-of-knowledge about the value of r is obtained by making the more pessimistic assumption that the four quoted error-bars only
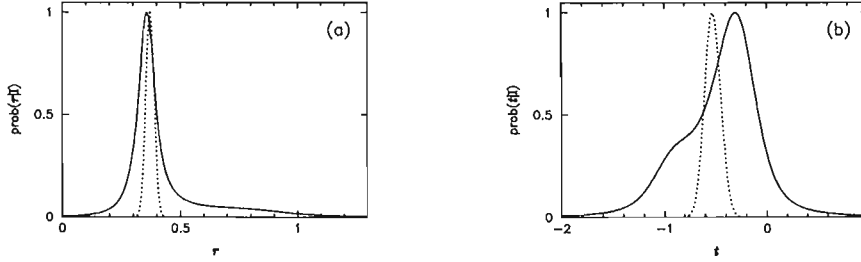
Figure 5. The solid lines show the p.d.f.'s representing our resultant knowledge of r and t given by several different pieces of information; being based on somewhat pessimistic assumptions, they are less constraining, and more realistic, than the equivalent conventional analysis indicated by the dotted lines. It should be noted that the p.d.f.'s are not normalized, but have been scaled to have a maximum of unity.

define a lower bound on the related uncertainties. Following this line of thought in a more formal[20] leads to the resultant probability density function (p.d.f.) for r shown by the solid curve in Fig. 5(a); for comparison, the implicit Gaussian p.d.f. pertaining to the conventional analysis mentioned earlier is shown with a dotted line. Although a value of r around 0.37 is still most probable, we are now not prepared to rule out the possibility that it may be of order unity quite so strongly.

A similar analysis of three values of t inferred from x-ray diffraction data $(-0.35 \pm 0.15, -1.00 \pm 0.13$ and $-0.19 \pm 0.13)$ leads to the resultant p.d.f. for t shown in Fig. 5(b). The pairs of "measurements" for ϕ $(66.1° \pm 2.1°$ and $75.7° \pm 1.8°)$, $< L_0 >_m$ (- 0.5 and $-0.8)$ and $< \Lambda_0 >_m / 3 < L_0 >_m$ $(0.00 \pm 0.05$ and $-0.06 \pm 0.01)$ were also combined in our "conservative" manner but, in these cases, the resulting p.d.f.'s were approximated by Gaussians defined by $\phi = 71° \pm 5°$, $< L_0 >_m = -0.65 \pm 0.20$ and $< \Lambda_0 >_m / 3 < L_0 >_m = -0.060 \pm 0.025$.

Our state of knowledge about the vandium wavefunction is then encapsulated in three-dimensional p.d.f. for the parameters a, b and d conditional on our "noisy constraints" on r, t, ϕ, $< L_0 >_m$ and $< \Lambda_0 >_m / 3 < L_0 >_m$, and all the implicit assumption and approximation, jointly labelled as I: prob(a, b, d | I). This can be computed numerically on a three-dimensional grid spanning the space $-1 \le a \le 1$, $-1 \le b \le 1$ and $-1 \le d \le 1$, as follows:

(i)   for each point, calculate r, t, ϕ, and so on, corresponding to the associated values of a, b and d;

(ii) read off the probabilities for those values of r, t, ϕ, etc., from Fig 5 and related graphs not shown;

(iii) assign the product of these probabilities to the grid-point being considered.

The result will be a 3-dimension grid for the likelihood of a, b and d which, with the assumption that we know nothing about the values of these parameters *a priori*, is proportional to the p.d.f., prob(a, b, d | I), that we seek.

Carrying out the analysis above, we found that there are four regions of high probability in our 3-dimension hypothesis-space. They are all symmetry-related in that the constraints of the data leave an ambiguity with regard to the signs of a, b and d.
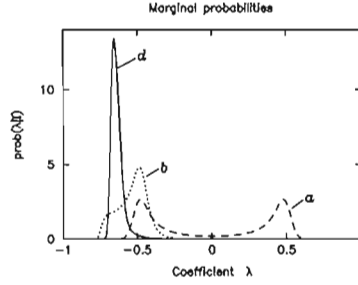
Figure 6. The marginal p.d.f.'s for a, b, and d, representing the constraints imposed on these expansion coefficients by our limited knowledge of r, t, ϕ, $<L_0>_m$ and $<\Lambda_0>_m/3 < L_0>_m$.

Since the absolute phase of the wavefunction is arbitrary, we choose to impose the condition $d \leq 0$. Due to a correlation between b and d, principally through the relationship $r = b/2d$, this restriction is sufficient to imply that $b \leq 0$, but the sign of a remains undetermined. The marginal probabilities for a, b and d are shown in Fig.6.

Given prob(a, b, d | I) we can make inferences about any quantity x, say, which is related to a, b and d, so that $x = $ f(a, b, d), by using the rules of probability theory:

$$\begin{aligned}
\text{prob}(x \mid \text{I}) &= \sum_{a,b,d} \text{prob}(x,a,b,d|\text{I}) \\
&= \sum_{a,b,d} \text{prob}(x|a,b,d,\text{I})\,\text{prob}(a,b,d|\text{I}) \\
&= \sum_{a,b,d} \delta(x - \text{f}(a,b,d))\,\text{prob}(a,b,d|\text{I})\,,
\end{aligned} \tag{13}$$

where δ is a Dirac delta-function. An example of such a calculation is illustrated in Fig.7, which shows the marginal probabilities for the real and imaginary part of the wavefunction expansion coefficient $c = c'+ic''$. While marginal p.d.f.'s are very useful for conveying our state-of-knowledge about one parameter irrespective of the others, they
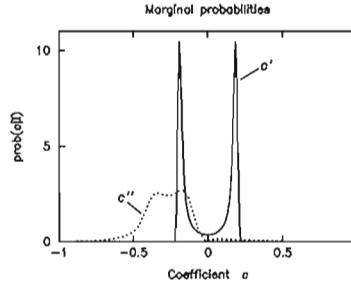

Figure 7. The marginal p.d.f.'s for the real and imaginary parts of the expansion coefficient c, inferred from our probabilistic analysis of the model wavefunction.

Table I. The table contains some values of orbital moments of the vanadium ion at site (1) in Fig.(1), with respect to orthogonal axes that include as components $\mathbf{a}_h = (a,0,0)$ and $\mathbf{c}_h = (0,0,c)$. Moments are proportional to an atomic tensor, namely, $\langle\mathbf{Q}\rangle = 3\sqrt{35/2}\ \langle\mathbf{T}^{(2)}\rangle$, $\langle\mathbf{\Lambda}\rangle = 3\sqrt{70}\ \langle\mathbf{T}^{(3)}\rangle$ and $\langle\mathbf{Y}\rangle = 18\sqrt{70}\ \langle\mathbf{T}^{(4)}\rangle$. Note that $\langle T_Q^{(K)}\rangle^* = (-1)^Q\langle T_{-Q}^{(K)}\rangle$. Values of the moments are derived from estimates of the coefficients in the model wavefunction given in Equ. (5).

$$\langle Q_0\rangle = 3\{3(b^2+d^2) + 4|c|^2\}/10 = 0.78 \pm 0.08$$

$$\langle Q_{+1}\rangle' = 3\{c'(d-b)\sqrt{2} - ab\sqrt{15}\}/10 = -0.25 \pm 0.06$$

$$\langle Q_{+2}\rangle'' = 3ac''/\sqrt{5} = 0.13 \pm 0.11$$

$$\langle \Lambda_0\rangle = 3(d^2-b^2-a^2) = -0.20 \pm 0.14$$

$$\langle \Lambda_{+1}\rangle' = -3c'(b+d) = 0.56 \pm 0.14$$

$$\langle \Lambda_{+2}\rangle'' = -3ac'' = -0.29 \pm 0.24$$

$$\langle \Lambda_{+3}\rangle = 3\sqrt{2}ad = 1.09 \pm 0.35$$

$$\langle Y_0\rangle = 6\{-7a^2 + b^2 + 6|c|^2 + d^2\} = 1.12 \pm 4.75$$

$$\langle Y_{+1}\rangle' = 6\sqrt{2}\{-4ab + c'(d-b)\sqrt{(15/2)}\} = -7.46 \pm 1.91$$

$$\langle Y_{+2}\rangle'' = 6\sqrt{3}\ ac'' = 1.02 \pm 0.83$$

$$\langle Y_{+3}\rangle = 6\sqrt{14}\ ad = 5.77 \pm 1.82$$

$$\langle Y_{+4}\rangle = 0.$$

do, of course, only give a partial picture of the situation. For example, they do not tell us the signs of a and c' are anticorrelated, so that $c' > 0$ if $a < 0$ and vice versa. To avoid this particular source of ambiguity, the remaining results in this paper assume that $a \leq 0$; the alternative choice, of $a \geq 0$, lead to equivalent symmetry-related conclusions.

Rather than displaying prob($x\,|\,$I), we often try to summarize its salient features by quoting a "best" estimate x_0 and a measure of its uncertainty σ (i.e. $x = x_0 \pm \sigma$); the most common practice is to use the mean, $x_0 = \langle x\rangle = \int x\ \text{prob}(x\,|\,\text{I})dx$, and the variance, $\sigma^2 = \langle (x-x_0)^2\rangle$. We have done this for some components of the quadrupole $\langle\mathbf{Q}\rangle$, octupole $\langle\mathbf{\Lambda}\rangle$ and hexadecapole $\langle\mathbf{Y}\rangle$ moments of the 3d valence shell of the V ion at site (1) in Fig.1. Our findings are summarized in Table I.

Looking at entries in Table I, it is evident that we have a good knowledge of all moments with the projections $Q = +1$ and $+3$, yet some moments with even Q are known very poorly, e.g. $\langle Y_0\rangle$. The estimates in Table I serve as tests to be met by an *ab initio* calculation of orbital properties of a vanadium ion in V_2O_3. Our inferred model wavefunction $|G\rangle$ is illustrated graphically in Fig.8. We display isosurfaces of $\langle|\langle\mathbf{r}|G\rangle|^2\rangle$, or the expected wavefunction when averaged over prob($a, b, d\,|\,$I). In addition, we provide two colour contour sections through the 3-dimension orbital density and its uncertainty equivalent.
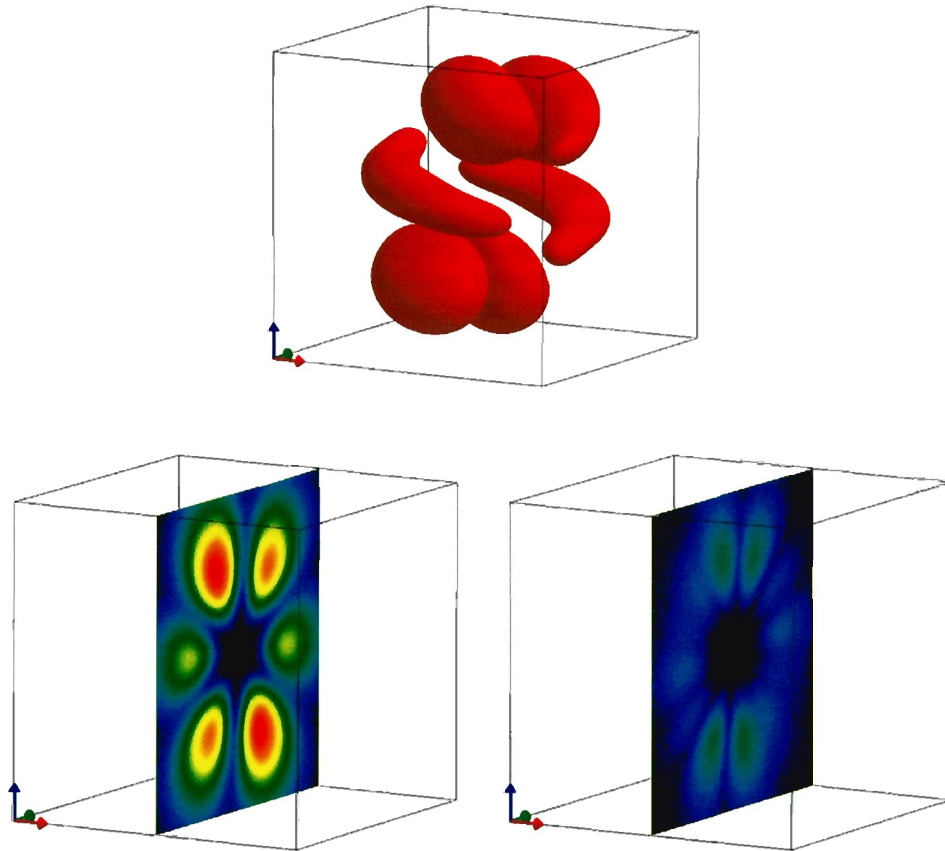
Figure 8. (a) An isosurface of the expected electron-density inferred from our probabilistic analysis of the model wavefunction. (b) An equivalent colour-contour slice through the 3-dimensional density, and (c) the corresponding 1-σ uncertainties displayed on the same scale. The red, green and blue arrows indicate the spatial x, y, and z axes of the crystal, respectively.

With regard to the nature of the ordering of orbital moments in the unit cell relevant information is contained in the relation between tensors for sites (1) and (7). (As before, we will use othogonal axes $(x, y\ z)$ with $x(z)$ parallel to $\mathbf{a}_h(\mathbf{c}_h)$.) Applied to the quadrupole moment one finds that, for the two sites in question $< Q_{yz} >$ and $< Q_{xx} - Q_{yy} >$ have one sign, whereas $< Q_{+1} >' \propto - < Q_{xz} >$ and $< Q_{+2} >'' \propto < Q_{xy} >$ are opposite in sign at the two sites. All diagonal atomic tensors $< T_0^{(K)} >$ are of one sign.

5. CONCLUSIONS

We have added a successful interpretation of Templeton-Templeton x-ray scattering to our earlier success with magnetic scattering by magnetically ordered V_2O_3. Expressed in terms of trigonal axes, that include $\mathbf{a}_h$ and $\mathbf{c}_h$, a vanadium ion in magnetically ordered

V_2O_3 bears an imprint of the three-fold rotation symmetry associated with the high-symmetry (corundum) structure adopted above the Néel temperature. In addition, the resonant x-ray Bragg diffraction data we have interpreted is consistent with an orbital magnetic moment confined to the plane $\mathbf{a}_m - \mathbf{c}_m$, which is normal to $\mathbf{a}_h = \mathbf{b}_m$, and inclined with respect to $\mathbf{c}_h$ by an angle $\phi \sim 70°$. However, resonant x-ray diffraction experiments are not suitable for the determination of the magnitude of the orbital moment. (The moment can be measured by diffraction of x-rays with an energy well above the resonance region or neutron diffraction.)

The successful outcome of our interpretation has been exploited to characterize orbital properties of a vanadium ion. To this end, we have used a model wavefunction created from the V ion ground state determined by Hund's rules. Coefficients in the model are determined by fitting to material properties that enter our interpretation of experimental date. One use of our inferred model wavefunction is to estimate orbital moments. The moments characterize the 3d valence shell and the ordering of orbitals in the magnetic unit cell.

Acknowledgements

REFERENCES

1.   D. B. McWhan, T. M. Rice, and J. P. Remeika, Phys. Rev. Lett. **23**, 1334 (1969).
2.   P. D. Dernier and M. Marezio, Phys. Rev. **B2**, 3771 (1970).
3.   R. M. Moon, Phys. Rev. Lett. **25**, 527 (1970).
4.   D. B. McWhan et al., Phys. Rev. **B7**, 1920 (1973).
5.   N. F. Mott, Metal-Insulator Transitions (Taylor and Francis, London, 1990)
6.   T. M. Rice, Spectroscopy of Mott Insulators and Correlated Metals, edited by A. Fujimori and Y. Tokura
         (Springer, Berlin, 1995).
7.   F. Mila et al., Phys. Rev. Lett. **85**, 1714 (2000).
8.   L. Paolasini et al., Phys. Rev. Lett. **82**, 4719 (1999).
9.   L. Paolasini et al., submitted to J. Elect. Spect. & Related Phenomena (2000).
10.   L. Paolasini, private communication.
11.   S. W. Lovesey and K. S. Knight, J. Phys.: Condens. Matter **12**, L367 (2000).
12.   D. H. Templeton and L. K. Templeton, Phys. Rev. **B49**, 14850 (1994).
13.   D. H. Templeton, Acta Cryst. **A54**, 158 (1998).
14.   K. D. Finkelstein, Q. Shen and S. Shastri, Phys. Rev. Lett. **69**, 1612 (1992).
15.   Y. Tanaka et al., J. Phys.: Condens. Matter **11**, L505 (1999).
16.   S. W. Lovesey, J. Phys.: Condens. Matter **10**, 2505 (1998).
17.   S. W. Lovesey, K. S. Knight and E. Balcar, to appear in Phys. Rev. **B** (2001).
18.   D. S. Sivia, Data Analysis – A Bayesian Tutorial (Oxford University Press, Oxford, 1996).
19.   J. A. Nelder and R. Mead, Computer J. **7**, 308 (1965).
20.   D.S. Sivia, Dealing with duff data, MaxEnt **96**, eds. M. Sears, V. Nedeljkovic, N.E. Pendock and, S.
         Sibisi, University of Witwatersand, Johannesburg, 1997.